

Nitrogen-Doped Titanate-Anatase Core–Shell Nanobelts with Exposed {101} Anatase Facets and Enhanced Visible Light Photocatalytic Activity

Zhigang Xiong and Xiu Song Zhao*

School of Chemical Engineering, The University of Queensland, St. Lucia, Brisbane, QLD 4072, Australia

S Supporting Information

ABSTRACT: Anatase TiO₂ with specifically exposed facets has been extensively studied for maximizing its photocatalytic activity. However, most previous preparation methods involve high-pressure processing and corrosive chemicals. Few works have been conducted on hierarchical composite nanostructures assembled from well-defined TiO₂ nanocrystals. Here, we report a facile method for the preparation of nitrogen-doped titanate-anatase core–shell nanobelts. Anatase nanorods with specifically exposed {101} facets were obtained from a simple evaporation-induced, self-assembly (EISA) process and coupled with another semiconductor photocatalyst. The composite material with improved visible-light-harvesting ability, high charge-hole mobility, and low electron–hole recombination exhibited high photocatalytic performance and stability. The results presented here will make significant contributions toward the development of delicate composite photocatalysts for photocatalytic water purification and solar energy utilization.

Semiconductor photocatalysts are finding increasing applications in hydrogen generation, solar energy utilization, and environmental remediation.¹ A titanium dioxide (TiO₂) photocatalyst, which is only active under UV light irradiation, can degrade a wide range of toxic and recalcitrant organic pollutants from water. But the overall efficiency is low because of the rapid recombination of electron–hole ($e^- - h^+$) pairs after excitation.² However, coupling TiO₂ with another semiconductor with matched energetic levels of valence band (VB) and conduction band (CB) favors the $e^- - h^+$ separation,^{1j,2b} consequently improving the quantum efficiency. Alternatively, doping TiO₂ with various foreign elements such as nitrogen,³ sulfur,^{1j,l} and carbon⁴ can extend its response to visible light. It is reported that the dopant introduces an intra-band-gap energy state and/or oxygen vacancies in the semiconductor,^{1j,4} leading to an enhanced activity under visible light irradiation.

Recently, engineering the morphology of TiO₂ with specifically exposed crystal facets has proved to be effective in tuning the photocatalytic performance.⁵ Yang et al. first demonstrated that uniform anatase single crystals with 47% {001} facets^{5d} displayed a superior photoactivity.^{5c} While Wu et al.^{5a} reported that crystal anatase nanobelts with dominant {101} facets exhibited a higher photoactivity than the nanosphere counterparts. By comparing the performance of

different facets, Cheng et al.^{5b} concluded that the true photoactivity order of anatase TiO₂ crystal is {010} > {101} > {001}. Although it seems that there are some contradictory interpretations concerning how the crystalline exposed facets of anatase affect the resulting photoactivity,^{5f,6} it is generally accepted that the {101} facets are more reductive than {001} facets,^{5e} which could act as possible reservoirs of the photogenerated electrons, yielding a highly reactive surface for the reduction of O₂ to superoxide radicals.^{5f} As a result, the reactivity of TiO₂ nanocrystals can be finely tailored by morphological control, and a great deal of research has been done to further optimize TiO₂ facets to improve its photocatalytic performance.^{5a,b,f,6} However, most of the preparations of TiO₂ crystals were carried out under high-pressure conditions and in the presence of corrosive chemicals,^{5,7} such as hydrofluoric acid,^{5d,7b,c} sodium hydroxide,^{5a} etc.

Herein, we report a facile approach to the preparation of a core–shell nanostructure composed of titanate platelets and anatase crystals with plenty of exposed {101} facets, which, after doping with nitrogen, exhibited excellent photoactivity under visible light irradiation. Titanate was chosen to couple with anatase because of the following rationales: (1) it possesses a layered structure consisting of TiO₆ octahedra sheets by sharing four edges similar to that of anatase crystals,⁸ which is believed to enable an intimate contact of the two semiconductors; (2) composites consisting of anatase and titanate have been proven to perform excellently in the photocatalytic degradation of organic pollutants;^{8a,b,e} (3) the length of titanate nanobelts is normally at the scale of several tens of micrometers,^{8d,e} thus enabling easy separation via filtration or sedimentation for recycling. Importantly, this is the first time it has been demonstrated that crystalline anatase with specifically exposed facets can be directly grown on another semiconductor through a simple evaporation-induced, self-assembly (EISA) process.⁹ We believe that the method described in this paper provides a simple yet effective route to rational design of delicate composite photocatalysts for applications beyond photocatalysis.

Figure 1 shows the XRD patterns of anatase, titanate, and a composite N–K₂Ti₄O₉–TiO₂ prepared in this work. The diffraction peaks of the titanate sample are in good accordance with that reported in the literature,^{8d} indicating the formation

Received: January 22, 2012

Published: March 22, 2012

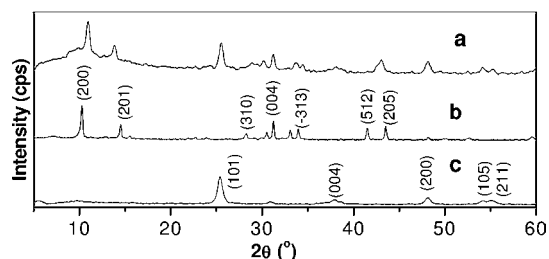


Figure 1. XRD patterns of $N\text{-K}_2\text{Ti}_4\text{O}_9\text{-TiO}_2$ (a), $\text{K}_2\text{Ti}_4\text{O}_9$ (b), and bulk anatase TiO_2 (c).

of the $\text{K}_2\text{Ti}_4\text{O}_9$ phase (JCPDS No. 32-0861). As a member of $\text{M}_2\text{O}\cdot n\text{TiO}_2$ ($M = \text{Na}, \text{K}, \text{Rb}, \text{Cs}$) with $n = 0.5, 1.0,$ or 2.0 ,^{8d} $\text{K}_2\text{Ti}_4\text{O}_9$ ($n = 4$) possesses a layered structure consisting of ribbons of edge- and corner-shared TiO_6 octahedra separated by K ions. After coupling with TiO_2 , the crystal phase of $\text{K}_2\text{Ti}_4\text{O}_9$ remained unchanged except for a slight broadening of the (200) peak, most probably due to intercalation of TiO_2 into the lamellar interlayer.^{8d} Other well-resolved peaks matching well with that of anatase (JCPDS No. 21-1272) are seen.^{1c} The sharp and intense peaks suggest a high crystallinity of the sample. Moreover, the width of the anatase diffraction peaks is narrower than that of other anatase samples synthesized using the template method,^{1c,h} indicating the formation of large TiO_2 particles in the present composite sample.

Figure 2 shows the FESEM/TEM images of different samples. It can be seen that $\text{K}_2\text{Ti}_4\text{O}_9$ consisted of nanobelts

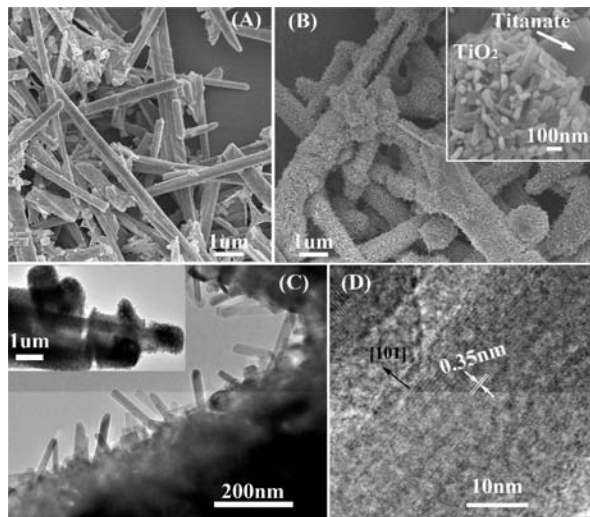


Figure 2. FESEM images of $\text{K}_2\text{Ti}_4\text{O}_9$ (A) and $N\text{-K}_2\text{Ti}_4\text{O}_9\text{-TiO}_2$ (B). TEM (C) and HRTEM images (D) of $N\text{-K}_2\text{Ti}_4\text{O}_9\text{-TiO}_2$.

of ~ 500 nm in thickness and up to several micrometers in length (Figure 2A). After coupling with TiO_2 , the thickness of the composite sample ($N\text{-K}_2\text{Ti}_4\text{O}_9\text{-TiO}_2$) increased to ~ 1.5 μm with rod-like anatase particles completely covering the surface of the titanate (Figure 2B). The anatase nanorods were $\sim 20\text{--}30$ nm in diameter and < 500 nm in length. The TEM images (Figure 2C) confirmed that the composite possessed a hierarchical core-shell structure with the anatase rods forming the shell around the titanate core (see the inset of Figure 2C). To identify the exposed facets of the nanorods, high-resolution TEM (HRTEM) was used to characterize the sample. As shown in Figure 2D, the lattice fringe along the [101] direction

clearly revealed the presence of the (101) plane with a lattice space of 0.35 nm. Considering the crystallographic symmetry of anatase nanorods, the dominant exposed facets can be identified as {101} planes, which are the most thermodynamically stable facets of anatase TiO_2 ,¹⁰ and constitute $\sim 95\%$ of the total exposed surface. The Brunauer-Emmett-Teller (BET) specific surface area of $N\text{-K}_2\text{Ti}_4\text{O}_9\text{-TiO}_2$ was determined to be ~ 15.4 m^2/g (Figure S1). The relatively low surface area is due to the large size of anatase nanorods and titanate platelets. However, the porous channel made by the assemblage of anatase solids would favor the transfer of organic pollutants from solution to the catalyst surface, benefiting heterogeneous reactions.

The photocatalytic performance of the as-synthesized composite photocatalyst was evaluated using the degradation of methylene blue (MB) under visible light irradiation. As shown in Figure 3, MB was very stable in the absence of light or

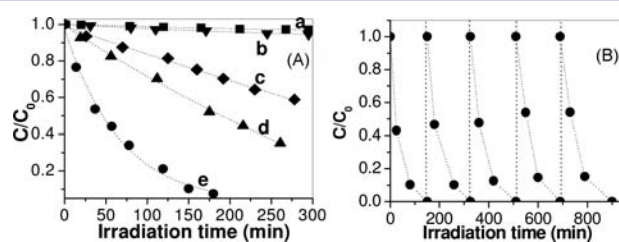


Figure 3. (A) Degradation of MB over catalyst without irradiation (a), under visible light without catalyst (b), over $\text{K}_2\text{Ti}_4\text{O}_9\text{-TiO}_2$ (c), P25 (d), or $N\text{-K}_2\text{Ti}_4\text{O}_9\text{-TiO}_2$ (e) under visible light irradiation. $[\text{MB}] = 1.1 \times 10^{-3}$ mM. (B) Repeated photocatalytic degradation of MB over $N\text{-K}_2\text{Ti}_4\text{O}_9\text{-TiO}_2$. $[\text{MB}] = 5.3 \times 10^{-4}$ mM.

a photocatalyst, which underwent slight degradation over visible-light-illuminated P25 or $\text{K}_2\text{Ti}_4\text{O}_9\text{-TiO}_2$ photocatalysts. In the presence of sample $N\text{-K}_2\text{Ti}_4\text{O}_9\text{-TiO}_2$, the removal rate was greatly enhanced with a rate constant of $\sim 1.4 \times 10^{-2}$ min^{-1} , nearly 4 times larger than that of P25 (3.6×10^{-3} min^{-1}). The absorption of MB in the visible light region gradually decreased with irradiation time (Figure S2A), indicating the complete destruction of aromatic structures. Compared to P25 that can only be excited by UV light and decompose dye pollutants via a photosensitization process,^{1h} composite $N\text{-K}_2\text{Ti}_4\text{O}_9\text{-TiO}_2$ demonstrated an improved photocatalytic performance. The photosensitized degradation caused by the excitation of MB might also be possible,^{1a} but its contribution could be neglected compared to the photocatalytic degradation.^{1h} To further identify the visible light activity of $N\text{-K}_2\text{Ti}_4\text{O}_9\text{-TiO}_2$, benzoic acid that has no absorption in the visible light region was used as a probe molecule, which underwent efficient degradation over the composite photocatalyst under visible light illumination (Figure S2B), but it was hardly removed by P25 or $\text{K}_2\text{Ti}_4\text{O}_9\text{-TiO}_2$ under the same experimental conditions. To reuse a photocatalyst, the photocatalyst must be easily separated from the reaction medium and maintain its activity. The composite material described in this paper displayed an extraordinary high stability and recyclability. It can be easily separated by simple sedimentation due to its large particle size (Figure S3). Moreover, even though the composite had been reused five times, it still exhibited high photoactivity (Figure 3B). The enhanced performance of $N\text{-K}_2\text{Ti}_4\text{O}_9\text{-TiO}_2$ could be attributed to its unique surface and electronic properties that substantially affected the photocatalytic processes involved in

the degradation, including generation of charge–hole pairs, transfer and trapping of charge carriers, and recombination of charge–hole pairs.

Figure 4 shows the UV–visible diffuse reflectance spectra of samples. $K_2Ti_4O_9$ had a strong absorption in the UV region.

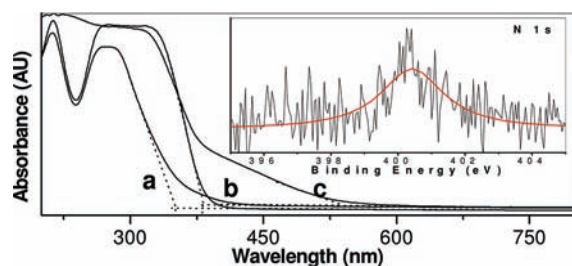


Figure 4. UV–visible reflectance spectra of $K_2Ti_4O_9$ (a), $K_2Ti_4O_9-TiO_2$ (b), and $N-K_2Ti_4O_9-TiO_2$ (c), and N 1s XPS spectrum of $N-K_2Ti_4O_9-TiO_2$ (inset).

After loading with anatase, the absorption edge of composite $K_2Ti_4O_9-TiO_2$ shifted from 351 (ca. 3.53 eV) to ~ 381 nm (ca. 3.3 eV) due to the narrow band gap of anatase (ca. 3.2 eV).^{1b} Doping with nitrogen (0.31 wt %) further extended the absorption to visible light with the wavelength ranging from 403 to 531 nm. Apparently, the nitrogen dopant promoted the light harvesting ability, while there is no red shift of the band edge and negligible absorption above 600 nm, indicating that the enhanced response to visible light is attributed not to the generation of oxygen vacancies, but to the nitrogen dopant, which introduced localized states near the top of the VB of TiO_2 or $K_2Ti_4O_9$.^{3c} The X-ray photoelectron spectrum of N 1s shown in Figure 4 confirmed the presence of the N element with a binding energy of ca. 400 eV, suggesting the interstitial incorporation of N species into the composite material and the formation of Ti–O–N or Ti–N–O oxynitride bonds.^{3d} It is noteworthy that due to the structural similarity of TiO_6 octahedra in TiO_2 and titanate, the nitrogen dopant is assumed to be localized in the crystal lattice of both TiO_2 and $K_2Ti_4O_9$.^{8a} In addition, considering that the energy potentials of the CB and VB of $K_2Ti_4O_9$ and TiO_2 are -0.48 and 3.06 , -0.53 , and 2.67 V, respectively,^{1b,8d} and the composite has a strong absorption below 531 nm (ca. 2.33 eV) (Figure 4), the highest potential of localized states introduced by the N dopant was calculated to be ~ 1.8 V, suggesting that both $K_2Ti_4O_9$ and TiO_2 were excited by visible light to generate e^-h^+ pairs (Figure 5A).

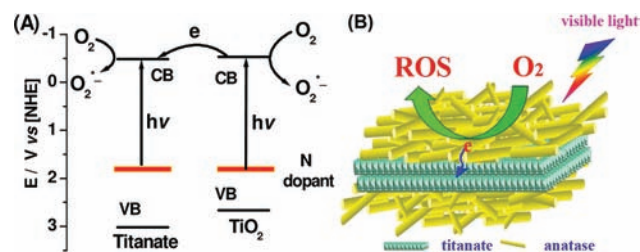


Figure 5. (A) Energy levels of titanate and anatase using normal hydrogen electrode (NHE) as reference at pH 7. The potential of TiO_2 CB band was calculated from $E_{CB} = -0.12 - 0.059$ pH. (B) Schematic illustration of the photocatalytic processes involved in the composite catalyst.

Transfer of photogenerated electrons and holes to the catalyst surface is one of the most critical processes in a photocatalytic reaction, as it governs the subsequent production of reactive oxygen species (ROS) and the resulting photocatalytic efficiency. The surface energy states, originated from the surface and bulk irregularities, which occur naturally during the preparation process,^{1f} usually lie in the midgap of semiconductors and are localized, serving as charge-carrier traps and impeding the migration of charge carriers to the reactive sites at the catalyst surface. However, anisotropically shaped particles, such as nanorods, nanobelts, and nanotubes, have been found to have a lower charge-carrier recombination rate.^{5e} Density functional theory (DFT) calculations indicated that TiO_2 nanobelts have less localized states near the band edges or in the band gap and possess an improved conductivity as compared to TiO_2 nanospheres.^{5a} Thus, the long anisotropically shaped titanate nanosheets and anatase nanorods are expected to inherently promote the efficient dissociation of e^-h^+ pairs and the transfer of charge carriers to different crystal facets.^{5e}

The dissociated e^-h^+ pairs could be trapped at the photocatalyst surface to generate various ROS for desired degradations in an aerated solution. It is reported that a great deal of organic or inorganic substrates could be degraded by oxidative species such as valence holes or hydroxyl radicals.^{1b} Some researchers reported that a surface-bound hydroxyl radical ($\bullet OH_{ads}$) is a key species for the oxidative reaction.¹¹ In the present study, the degradation rate of MB over composite $N-K_2Ti_4O_9-TiO_2$ showed a great decrease in the presence of benzoquinone or ethanol (Figure S4), which are scavengers of $O_2^{\bullet-}$ or $\bullet OH$, respectively,¹² with rate constants of about 6.1×10^{-3} and $1.1 \times 10^{-2} \text{ min}^{-1}$, clearly indicating the involvement of ROS in the MB degradation process with $\sim 56\%$ of MB removed by $O_2^{\bullet-}$. This has also been observed from other photocatalytic systems containing TiO_2 crystals with specifically exposed $\{101\}$ facets.^{5a,f} Wu et al.^{5a} reported that crystal anatase nanobelts with dominant $\{101\}$ facets displayed higher photoactivity than nanospheres due to the generation of more $O_2^{\bullet-}$ on the catalyst surface. Using electron spin resonance spectroscopy, D' Arienzo et al.^{5e} observed that the trapped electrons increased with the specific surface area of $\{101\}$ facets. Employing a single-molecule fluorescence technique, Tachikawa and co-workers^{5f} also discovered that the $\{101\}$ facets are more reductive than the $\{001\}$ facets, which act as possible reservoirs of the photogenerated electrons and facilitate the production of superoxide radicals.^{5a} In the present work, it is difficult to relate all $O_2^{\bullet-}$ to the presence of $\{101\}$ anatase facets, but the anatase nanorods with dominant exposed $\{101\}$ facets are believed to play a significant role in the enhanced degradation of MB (Figure 3A).

It has been reported that most of the charge carriers of a photoexcited TiO_2 photocatalyst recombine in less than 10 ns, leading to rapid depletion of photogenerated carriers.^{2b} It has also been shown that coupling of TiO_2 with another semiconductor with an adequately matched band structure could physically separate the charge carriers upon generation, therefore greatly decreasing the recombination rate.^{1j} The fate of photoexcited charge carriers can be characterized by photoluminescence (PL) spectroscopy, as the emission represents the direct band gap, indirect band gap, or defect-mediated recombinations.¹³ Supra-band-gap irradiation of TiO_2 results in emission at wavelengths spanning from 350 to 650 nm (Figure S5). In composite $K_2Ti_4O_9-TiO_2$, the PL

quenching was observed at the range of 400–500 nm compared to that of TiO₂ (Figure S5), indicating the possible lower energy indirect band gap and trap-level-mediated transitions.¹³ The coupling between titanate and anatase indeed retarded the e^-h^+ recombination. As shown in Figure 5A, although the potential difference of the CB between titanate and anatase is insignificant, the potential gap could still act as a driving force for the continuous electron transfer from the CB of anatase to that of titanate (Figure 5B), which improved the utilization of charge carriers and ultimately enhanced the MB degradation rate.

In conclusion, a novel composite photocatalyst, N–K₂Ti₄O₉–TiO₂, with a core–shell hierarchical structure has been prepared. Anatase TiO₂ nanorods with specifically exposed facets were directly obtained through a simple EISA method and mounted on the external surface of titanate platelets. The composite showed high visible-light-responding ability, excellent e^-h^+ mobility, and low e^-h^+ recombination, and therefore demonstrated superior photocatalytic activity and stability.

■ ASSOCIATED CONTENT

● Supporting Information

Experimental details, N₂ sorption isotherm curves, absorption spectra of MB and benzoic acid, sedimentation images, degradation curves, and photoluminescence spectra. This material is available free of charge via the Internet at <http://pubs.acs.org>.

■ AUTHOR INFORMATION

Corresponding Author

george.zhao@uq.edu.au

Notes

The authors declare no competing financial interest.

■ ACKNOWLEDGMENTS

Australian Research Council (ARC) is acknowledged for supporting the work under the ARC Future Fellow Program (FT100100879).

■ REFERENCES

- (1) (a) Chen, C. C.; Ma, W. H.; Zhao, J. C. *Chem. Soc. Rev.* **2010**, *39*, 4206. (b) Tachikawa, T.; Fujitsuka, M.; Majima, T. *J. Phys. Chem. C* **2007**, *111*, 5259. (c) Xiong, Z.; Dou, H.; Pan, J.; Ma, J.; Xu, C.; Zhao, X. S. *CrystEngComm* **2010**, *12*, 3455. (d) Chen, X.; Shen, S.; Guo, L.; Mao, S. S. *Chem. Rev.* **2010**, *110*, 6503. (e) Hoffmann, M. R.; Martin, S. T.; Choi, W. Y.; Bahnemann, D. W. *Chem. Rev.* **1995**, *95*, 69. (f) Linsebigler, A. L.; Lu, G. Q.; Yates, J. T. *Chem. Rev.* **1995**, *95*, 735. (g) Xu, Y.; Lv, K.; Xiong, Z. G.; Leng, W.; Du, W.; Liu, D.; Xue, X. *J. Phys. Chem. C* **2007**, *111*, 19024. (h) Xiong, Z. G.; Ma, J. Z.; Ng, W. J.; Waite, T. D.; Zhao, X. S. *Water Res.* **2011**, *45*, 2095. (i) Fujishima, A.; Zhang, X. T.; Tryk, D. A. *Surf. Sci. Rep.* **2008**, *63*, 515. (j) Zhang, H. J.; Chen, G. H.; Bahnemann, D. W. *J. Mater. Chem.* **2009**, *19*, 5089. (k) Tahiri, H.; Serpone, N.; LevanMao, R. *J. Photochem. Photobiol. A* **1996**, *93*, 199. (l) Han, C.; Pelaez, M.; Likodimos, V.; Kontos, A. G.; Falaras, P.; O'Shea, K.; Dionysiou, D. D. *Appl. Catal., B* **2011**, *107*, 77.
- (2) (a) Skinner, D. E.; Colombo, D. P.; Cavaleri, J. J.; Bowman, R. M. *J. Phys. Chem.* **1995**, *99*, 7853. (b) Mukherji, A.; Seger, B.; Lu, G. Q.; Wang, L. *ACS Nano* **2011**, *5*, 3483.
- (3) (a) D'Arienzo, M.; Siedl, N.; Sternig, A.; Scotti, R.; Morazzoni, F.; Bernardi, J.; Diwald, O. *J. Phys. Chem. C* **2010**, *114*, 18067. (b) Mitoraj, D.; Kisch, H. *Angew. Chem., Int. Ed.* **2008**, *47*, 9975. (c) Lin, Z. S.; Orlov, A.; Lambert, R. M.; Payne, M. C. *J. Phys. Chem. B* **2005**, *109*, 20948. (d) Wang, J.; Tafen, D. N.; Lewis, J. P.; Hong, Z. L.

Manivannan, A.; Zhi, M. J.; Li, M.; Wu, N. Q. *J. Am. Chem. Soc.* **2009**, *131*, 12290.

(4) Dong, F.; Wang, H. Q.; Wu, Z. B. *J. Phys. Chem. C* **2009**, *113*, 16717.

(5) (a) Wu, N. Q.; Wang, J.; Tafen, D.; Wang, H.; Zheng, J. G.; Lewis, J. P.; Liu, X. G.; Leonard, S. S.; Manivannan, A. *J. Am. Chem. Soc.* **2010**, *132*, 6679. (b) Pan, J.; Liu, G.; Lu, G. M.; Cheng, H. M. *Angew. Chem., Int. Ed.* **2011**, *50*, 2133. (c) Yang, H. G.; Liu, G.; Qiao, S. Z.; Sun, C. H.; Jin, Y. G.; Smith, S. C.; Zou, J.; Cheng, H. M.; Lu, G. Q. *J. Am. Chem. Soc.* **2009**, *131*, 4078. (d) Yang, H. G.; Sun, C. H.; Qiao, S. Z.; Zou, J.; Liu, G.; Smith, S. C.; Cheng, H. M.; Lu, G. Q. *Nature* **2008**, *453*, 638. (e) D'Arienzo, M.; Carbajo, J.; Bahamonde, A.; Crippa, M.; Polizzi, S.; Scotti, R.; Wahba, L.; Morazzoni, F. *J. Am. Chem. Soc.* **2011**, *133*, 17652. (f) Tachikawa, T.; Yamashita, S.; Majima, T. *J. Am. Chem. Soc.* **2011**, *133*, 7197. (g) Pan, J.; Wu, X.; Wang, L.; Liu, G.; Lu, G. Q.; Cheng, H.-M. *Chem. Commun.* **2011**, *47*, 8361.

(6) Murakami, N.; Kurihara, Y.; Tsubota, T.; Ohno, T. *J. Phys. Chem. C* **2009**, *113*, 3062.

(7) (a) Han, X. G.; Kuang, Q.; Jin, M. S.; Xie, Z. X.; Zheng, L. S. *J. Am. Chem. Soc.* **2009**, *131*, 3152. (b) Liu, G.; Yu, J. C.; Lu, G. Q.; Cheng, H. M. *Chem. Commun.* **2011**, *47*, 6763. (c) Liu, S. W.; Yu, J. G.; Jaroniec, M. *Chem. Mater.* **2011**, *23*, 4085.

(8) (a) Cheng, Y. H.; Huang, Y. Z.; Kanhere, P. D.; Subramaniam, V. P.; Gong, D. G.; Zhang, S.; Highfield, J.; Schreyer, M. K.; Chen, Z. *Chem.—Eur. J.* **2011**, *17*, 2575. (b) Zhu, H. Y.; Lan, Y.; Gao, X. P.; Ringer, S. P.; Zheng, Z. F.; Song, D. Y.; Zhao, J. C. *J. Am. Chem. Soc.* **2005**, *127*, 6730. (c) Liu, G.; Wang, L. Z.; Sun, C. H.; Yan, X. X.; Wang, X. W.; Chen, Z. G.; Smith, S. C.; Cheng, H. M.; Lu, G. Q. *Chem. Mater.* **2009**, *21*, 1266. (d) Allen, M. R.; Thibert, A.; Sabio, E. M.; Browning, N. D.; Larsen, D. S.; Osterloh, F. E. *Chem. Mater.* **2010**, *22*, 1220. (e) Zhu, H. Y.; Gao, X. P.; Lan, Y.; Song, D. Y.; Xi, Y. X.; Zhao, J. C. *J. Am. Chem. Soc.* **2004**, *126*, 8380.

(9) Brinker, C. J.; Lu, Y. F.; Sellinger, A.; Fan, H. Y. *Adv. Mater.* **1999**, *11*, 579.

(10) (a) Lazzeri, M.; Vittadini, A.; Selloni, A. *Phys. Rev. B* **2001**, *63*, 155409. (b) Dai, Y. Q.; Cobley, C. M.; Zeng, J.; Sun, Y. M.; Xia, Y. N. *Nano Lett.* **2009**, *9*, 2455.

(11) Mao, Y.; Schoeneich, C.; Asmus, K. D. *J. Phys. Chem.* **1991**, *95*, 10080.

(12) Xiong, Z. G.; Zhang, L. L.; Zhao, X. S. *Chem.—Eur. J.* **2011**, *17*, 2428.

(13) Liang, Y. T.; Vijayan, B. K.; Gray, K. A.; Hersam, M. C. *Nano Lett.* **2011**, *11*, 2865.